STEM CELLS TRANSLATIONAL MEDICINE®

PROTOCOLS AND MANUFACTURING FOR CELL-BASED THERAPIES

Directed Differentiation of Human Embryonic Stem Cells Toward Placode-Derived Spiral Ganglion-Like Sensory Neurons

AKIHIRO J. MATSUOKA,[a,b,c] ZACHERY D. MORRISSEY,[a] CHAOYING ZHANG,[a] KAZUAKI HOMMA,[a,c] ABDELHAK BELMADANI,[d] CHARLES A. MILLER,[a] DUNCAN M. CHADLY,[a] SHUN KOBAYASHI,[a] ALEXANDRA N. EDELBROCK,[e] MIHO TANAKA-MATAKATSU,[a] DONNA S. WHITLON,[a,c] LJUBA LYASS,[e] TAMMY L. MCGUIRE,[e] SAMUEL I. STUPP,[e,f,g,h,i] JOHN A. KESSLER[j]

Key Words. Embryonic stem cells • Cellular therapy • Neural differentiation • Stem cell • Transplantation • Neural induction • Progenitor cells

[a]Department of Otolaryngology and Head and Neck Surgery, [d]Department of Molecular Pharmacology and Biological Chemistry, [g]Department of Medicine, [j]Department of Neurology, Feinberg School of Medicine, Northwestern University; [b]Department of Communication Sciences and Disorders, [c]Knowles Hearing Center, [e]Department of Biomedical Engineering, [f]Simpson Querrey Institute for BioNanotechnology, Chicago, IL, USA, [h]Department of Chemistry, [i]Department of Materials Science & Engineering, Northwestern University

Correspondence: Akihiro J. Matsuoka, M.D., D.M.Sc., Ph.D. 676 N. St. Clair Street Suite 1325 Chicago, Illinois 60611, USA. Telephone: 312-695-4995; Fax: 312-695-3194; e-mail: amatsuok@nm.org

Received 16 January 2016; accepted for publication 19 October 2016; published Online First on 10 December 2016.

1066-5099/2016/$30.00/0

http://dx.doi.org/10.1002/sctm.16-0032

ABSTRACT

The ability to generate spiral ganglion neurons (SGNs) from stem cells is a necessary prerequisite for development of cell-replacement therapies for sensorineural hearing loss. We present a protocol that directs human embryonic stem cells (hESCs) toward a purified population of otic neuronal progenitors (ONPs) and SGN-like cells. Between 82% and 95% of these cells express SGN molecular markers, they preferentially extend neurites to the cochlear nucleus rather than nonauditory nuclei, and they generate action potentials. The protocol follows an in vitro stepwise recapitulation of developmental events inherent to normal differentiation of hESCs into SGNs, resulting in efficient sequential generation of nonneuronal ectoderm, preplacodal ectoderm, early prosensory ONPs, late ONPs, and cells with cellular and molecular characteristics of human SGNs. We thus describe the sequential signaling pathways that generate the early and later lineage species in the human SGN lineage, thereby better describing key developmental processes. The results indicate that our protocol generates cells that closely replicate the phenotypic characteristics of human SGNs, advancing the process of guiding hESCs to states serving inner-ear cell-replacement therapies and possible next-generation hybrid auditory prostheses. © STEM CELLS TRANSLATIONAL MEDICINE *2017;6:923–936*

SIGNIFICANCE STATEMENT

The regeneration of auditory neurons (AN) would be highly useful in the treatment of sensorineural hearing loss (SNHL), but stem cell therapies for generating ANs have been limited to animal models, which are unsuitable for clinical applications. Here is presented a protocol for deriving a purified population of otic neuronal progenitors and AN-like cells from human embryonic stem cells. This study further shows that these AN-like cells express appropriate markers, preferentially extend neurites into the cochlear nucleus rather than to other brainstem nuclei, and can generate action potentials. This work represents a significant step in understanding human SGN development and in developing stem cell therapy for SNHL.

INTRODUCTION

Approximately 360 million people have disabling hearing losses [1], a number likely to grow due to increasing noise pollution and human longevity. The most common impairment is sensorineural hearing loss (SNHL). Stem-cell replacement of spiral ganglion neurons (SGNs) may effectively treat SNHL, motivating efforts for differentiating pluripotent stem cells (PSCs) into glutamatergic sensory neurons similar to SGNs [2–5]. Clinical translation of these findings faces hurdles, including developing efficient protocols, accurate reproduction of phenotypic characteristics of human SGNs, delivery and creation of supportive niches, confirmation of normal physiology of SGNs and ascending neural stages, and ultimately, restoration of hearing. This paper primarily addresses the first two hurdles and presents some SGN-level physiological findings.

A simplified model of SGN lineage indicates that PSCs first give rise to nonneuronal ectoderm (NNE), which develops into preplacodal ectoderm (PPE) [6]. PPE then becomes cranial placodes, including the otic placode, which contains SGN precursors [6]. Although developmental pathways governing commitment of precursor cells to

human SGNs are not completely understood, substantial insight has been provided by studies of chick, *Xenopus*, and rodent nervous systems and recent studies of human embryonic stem cells (hESCs) [7]. Inhibition of TGF-β signaling in cultured human and mouse ESCs increases efficiency of ectoderm generation [8, 9], which is biased to NNE fates by bone morphogenetic protein 4 (BMP4) signaling [10, 11]. Thus, subsequent inhibition of BMP signaling and activation of FGF pathways are essential to selectively differentiate NNE into PPE [12–14]. Wnt signaling limits lateral and posterior extents of the preplacodal region, inhibiting PPE differentiation [15]; transient Wnt inhibition helps create a PPE lineage [16]. Subsequent combined Wnt and FGF signaling is required to generate the otic placode and suppress other epibranchial placode domains [17–20] and insulin-like growth factor-1 (IGF-1) supports survival and proliferation of early otic vesicles [21–24]. These observations suggest that FGF, Wnt, and IGF-1 signaling are primary inducers of the otic placode. In vivo, the otic placode invaginates into mesenchyme to form the otic vesicle. Its ventral region contains prosensory otic neuronal progenitors (ONPs) that give rise to primary sensory neurons, including SGNs. Sonic Hedgehog (SHH) is required for ventral patterning of the inner ear in mice and acts synergistically with all-trans retinoic acid (ATRA) to facilitate otic sensory neuronal differentiation [25, 26].

We hypothesized that in vitro stepwise recapitulation of these developmental events efficiently facilitates differentiation of hESCs into SGNs. We define a protocol that efficiently generates cells that display phenotypic characteristics of SGNs and preferentially innervate the appropriate cochlear nucleus (CN) target in organotypic rat brainstem slice cocultures containing CN and ONPs. Our approach offers the advantage of discrete subprotocols, each of which can be further improved. The protocol was evaluated using multiple approaches. At key stages along its 42-63 day extent, outcomes were evaluated using immunocytochemistry, RT-PCR, and the rat ONP/CN coculture. Although not the focus of protocol development and evaluation, we also conducted physiological assessments on SGN-like cells.

Materials and Methods

See Supporting Information for details of all procedures and reagents and Figure 1 for the schematized protocol.

Development Stage 1: Generation of NNE-Like and PPE-Like Cells

Human ESC lines H1, H7, and H9 (passages 25-35; WiCell Research Institute, Madison, Wisconsin, USA, https://www.wicell.org) were cultured as previously described [27]. The step-wise processing is shown diagrammatically in Figure 1. Prior to differentiation, hESCs were purified using an Anti-TRA-1-60 MicroBead Kit, Feeder Removal Microbeads (mouse), LS Columns, and a MidiMACS Separator (Miltenyi Biotec, Bergisch Gladbach, Germany, http://www.miltenyibiotec.com). Single-suspended cells were plated on Geltrex (ThermoFisher Scientific, Waltham, MA, USA, http://www.thermofisher.com) coated plates either in Essential 8 medium (E8, ThermoFisher Scientific, Waltham, MA, USA) or mTeSR (STEMCELL Techonologies, Cambridge, MA, USA, https://www.stemcell.com) with Rho kinase inhibitor Y27632 (10 μM) for 48 hours at 10,000 cells cm^{-2}; this density minimizes differentiation toward central nervous system (CNS) neurons [8].

Differentiation toward NNE lineage was initiated 72 hours at day 3 (D3, Fig. 1) after seeding by changing medium from E8 to a chemically defined medium containing N2 and B27 supplements (N2B27-CDM) [14, 28] and adding 10 ng ml^{-1} recombinant BMP4, 1 μM SB431542, and 10 ng ml^{-1} recombinant human FGF2 for 3 days.

Differentiation toward PPE lineage was initiated at D6 (Fig. 1) by adding 2 μM IWP-2 along with dual SMAD signal inhibition [29] (1 μM SB431542 and 100 nM of LDN-193189 for 5 days). Cells were positively selected for $p75^{NTR}$ and negatively selected for TRA-1-81 using "gentle" fluorescence activated cell sorting (FACS) [30] with a FACS Aria SORP 4/5-Laser. Alternatively, a MACS neural stem cell microbead kit along with the Anti-TRA-1-60 MicroBead Kit, LS Columns, and a MidiMACS Separator was used to positively select cells for $p75^{NTR}$ and negatively select for TRA-1-60 [31].

Development Stage 2: ONP Generation

After purification at day 11, cells were seeded at 25,000 cells cm^{-2} on 12 mm coverslips maintained in N2B27-CDM with 100 ng ml^{-1} human Wnt3a, 10 ng ml^{-1} human FGF2, and 50 ng ml^{-1} IGF-1 (W/F/I), initiating the "early-stage ONP" epoch (D11-D16, Fig. 1). The "mid-stage ONP" epoch, initiated at D16, included two additional W/F/I days followed by 3-day treatment with 500 ng ml^{-1} SHH, 0.5 μM ATRA, 10 ng ml^{-1} human FGF2, 20 ng ml^{-1} EGF, and 50 ng ml^{-1} IGF-1 (S/R/E/F/I) in N2B27-CDM. The "late-stage ONP" epoch began at D21 with four additional days of S/R/E/F/I treatment (Fig. 1). Some cells were maintained in ONP maintenance medium (ONPMM) before further sensory neuronal differentiation.

Development Stage 3: Sensory Neuronal Differentiation (SGN-Like Cells)

Neuronal differentiation toward SGNs was initiated using a neuronal induction medium (NIM) supplemented with 0.5 mM of dibutyryl-cyclic AMP (db-cyclic AMP), 10 ng ml^{-1} human brain-derived neurotrophic factor (BDNF), 10 ng ml^{-1} human neurotrophin-3 (NT-3), and 10 ng ml^{-1} IGF-1. Alternatively, BrainPhys Neuronal Medium and N2-A/SM1 (Stemcell Technologies Inc., Cambridge, MA) supplemented with 0.5 mM db-cyclic AMP, 20 ng ml^{-1} BDNF, 20 ng ml^{-1} NT-3, 20 ng ml^{-1} IGF-1, and 1 mM Glutamax was used (see Supporting Information). Both media yielded morphologically and immunocytochemically similar cells. Cells were cultured on 10 mm coverslips in 12-well culture dishes. Coverslips were first coated with poly-ornithine (0.1 mg ml^{-1} in 10 mM borate buffer, pH 8.4) for 1 hour at room temperature followed by laminin at 20 μg ml^{-1} in HBSS at 4°C overnight. Cells seeded at 10,000-25,000 cells cm^{-2} were allowed to grow 4-6 weeks, with medium changes every 3 days.

Reverse Transcription and Polymerase Chain Reaction

RNA extraction and real-time reverse transcriptase PCR (RT-PCR) were performed using standard techniques.

Immunocytochemistry, Image Acquisition, Cell Viability, and Quantification

Immunocytochemistry employed standard techniques [32, 33]. Secondary-antibody-only controls were performed by omitting primary antibodies during incubation (see Supporting Information). Fluorescent imaging was performed on a Zeiss UV-LSM 510 META and a Nikon A1 confocal microscope. Sequential scanning of channels was performed to prevent false-positive

Stem Cells Translational Medicine published by Wiley Periodicals, Inc. on behalf of AlphaMed Press

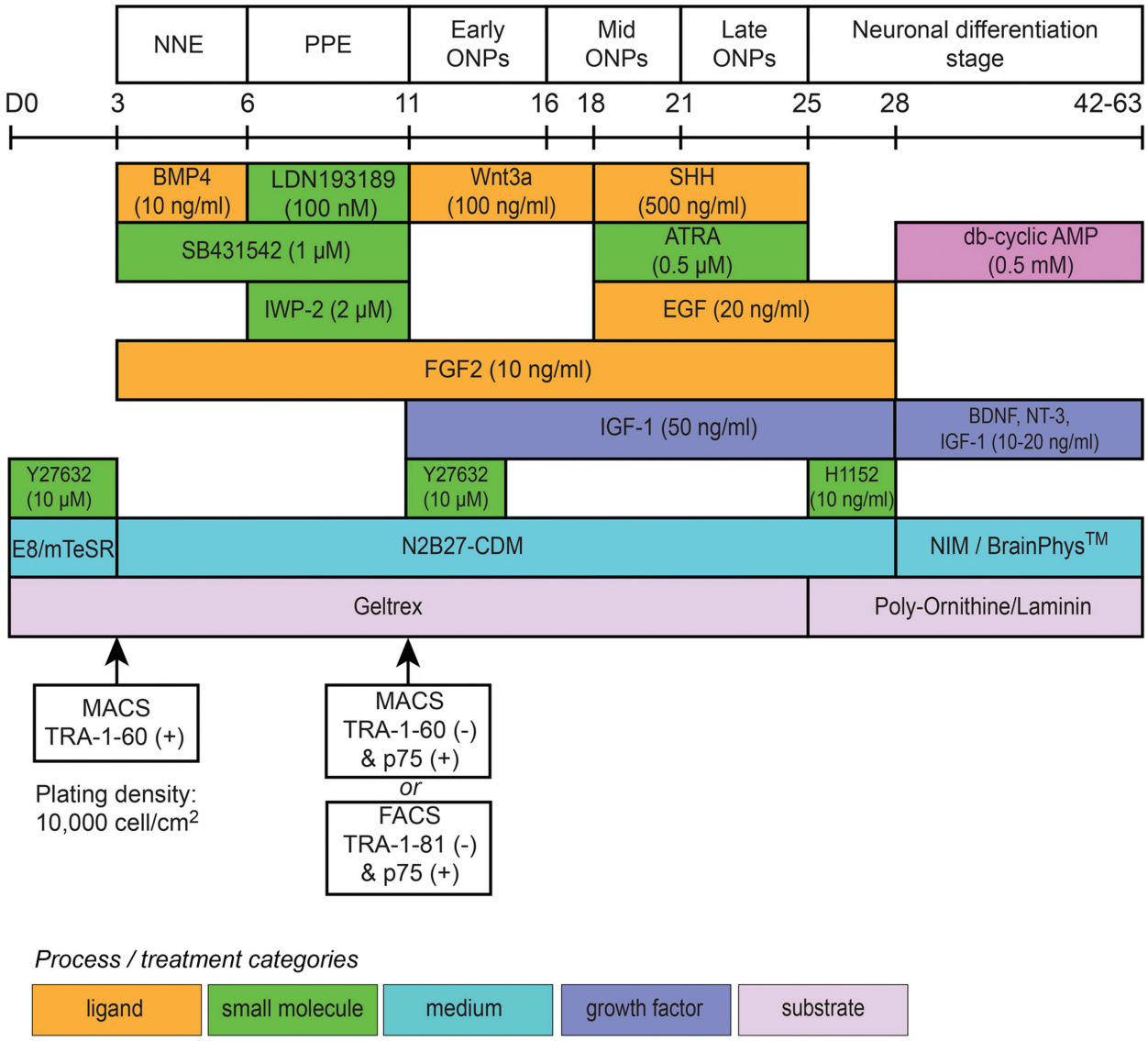

Figure 1. Schematic summary of the stepwise treatment protocol for deriving the spiral ganglion neurons lineage from undifferentiated H1, H7, and H9 human embryonic stem cells lines. Developmental stages are shown at top, below that a timeline, and key processes are shown below that, using color-coded bars. Abbreviations: ATRA, all-trans retinoic acid; BDNF, brain derived neurotrophic factor; BMP4, bone morphogenetic protein 4; D: days; E8: Essential 8 medium; EGF, epidermal growth factor; FACS, fluorescence activated cell sorting; FGF2, fibroblast growth factor 2; IGF-1, insulin-like growth factor 1; IWP-2, Wnt pathway inhibitor; MACS, magnetic activated cell sorting; N2B27-CDM, N2B27 chemically defined medium; NIM, neuronal induction medium; NNE, nonneuronal ectoderm; NT3, neurotrophin 3; ONP, otic neuronal progenitor; p75, low-affinity neurotrophin receptor ($p75^{NTR}$); PPE, preplacodal ectoderm; SHH, Sonic hedgehog.

colocalization. Images were quantified using ImageJ. Cell viability was assessed using a 3-(4,5-dimethylthiazol-2yl)-2,5 diphenyl tetra-zolium bromide (MTT) Cell Proliferation Assay Kit [34].

Electrophysiological Assessments

Three approaches were used to assess physiological responses of SGN-like cells: (a) calcium imaging [32], (b) whole-cell recordings of hESC-derived neurons, using an Axopatch 200A amplifier and standard cell-clamp approaches, and (c) a voltage-sensitive dye (VSD) to noninvasively assess electrically evoked cell depolarization consistent with neuronal activity, following established protocol [35] and further outlined in the Supporting Information.

The Organotypic Rat Brainstem Slice Culture With hESC-Derived ONPs

We developed a coculture consisting of an ONP aggregate and rat CN within a brainstem slice to study directed neurite growth and connectivity. The organotypic brainstem slice protocol has been described elsewhere [36, 37] and in the Supporting Information. Brainstem slices containing the nucleus of the solitary tract (NST) near the middle olive were also cocultured as controls to evaluate the specificity of neurite extension to the CN. ONPs within a collagen gel sphere or a self-assembling peptide amphiphile bearing an IKVAV epitope (IKVAV-PA [38]) were positioned 750 μm from the CN or NST 4 days after

beginning the brainstem slice culture (Supporting Information Fig. 2D). We first evaluated ONP survival in these gel spheres using MTT cell viability proliferation assay (Supporting Information Fig. 2E). At days 14 and 28, significantly better ONP survival was observed in the IKVAV-PA gel; we subsequently used only IKVAV-PA cocultures.

Statistical Analyses

Statistical analysis was performed with one-way ANOVA (with Tukey post hoc test) or two-tailed, unpaired Student's *t* test with or without Welch's modification [39], as indicated. Values are typically expressed as mean ± standard error.

Results

Evaluation of hESC-Derived SGN-Like Cells

Stage 1: hESC-Derived NNE-Like and PPE-Like Cells. Within the NNE epoch (initiated at D3), treatment duration was optimized for efficiency using immunocytochemistry for AP2α and DLX3 (NNE markers [40, 41]). Figures 2B and 2C indicate that 3-day treatment with BMP4/FGF2 (labeled "B/F") or BMP4/SB431542/FGF2 ("B/SB/F") sufficed for expression of AP2α and DLX3 in >90% of cells. We also evaluated possible aberrant differentiation into mesoendoderm using immunocytochemistry for Brachyury [9]. B/SB/F treatment markedly suppressed Brachyury expression compared with B/F or N2B27-CDM-only treatment (Fig. 2D). Human ESC morphology before (Fig. 2E(a)) and after B/SB/F treatment (at D1 in Fig. 2E(b) and D5 in Fig. 2E(c)) demonstrated changes from round to spindle-like shapes (also Supporting Information Fig. 1A). In adherent monolayer cultures, differentiation usually was initiated at the colony's outer border (white arrowheads, Fig. 2E(b)). Figure 2F shows immunocytochemistry for DLX3, DLX5, GATA2, and AP2α (markers for NNE [42]), indicating high conversion efficiency from undifferentiated hESCs into NNE.

At D6, treatment of NNE-like cells with dual SMAD signal inhibition (LDN193189 or Noggin + SB431542), FGF2, and Wnt antagonist IWP-2 to differentiate into PPE lineage (Figs. (1 and 2)G). We determined the effectiveness of PPE lineage induction by quantitative immunocytochemistry for EYA1 and SIX4, known PPE markers [40, 41], after 3, 5, 7, and 14 days of treatment. NNE-like cells were also cultured in N2B27-CDM only (control) condition. After 5 treatment days (i.e., D11), immunocytochemical staining for EYA1 and SIX4 exceeded 85% with Noggin (Noggin/SB/F/I) or LDN193189 (LDN/SB/F/I) (Figs. 2H, 2I). Noggin/SB/F/I and LDN/SB/F/I were equally effective in inducing the PPE lineage. We then quantified the PPE-like cells still expressing marker for undifferentiated hESCs (OCT3/4; Fig. 2J, left). LDN/SB/F/I treatment for 5 days significantly reduced OCT3/4 expression from 45.3% with N2B27-CDM-only treatment to 17.3% (Fig. 2J, left) ($p < .01$). During otocyst stages, $p75^{NTR}$ is expressed in identifiable domains of otic epithelium, surrounding mesenchyme, and cochleovestibular ganglion. During late embryogenesis, it is found more specifically in the cochleovestibular ganglion [43]. LDN/SB/F/I treatment for 5 days (Fig. 2J, right) significantly increased the rate of $p75^{NTR}$ expression from 50.1% to 73.3% ($p < .001$). As noted below, because of these heterogeneities, we subsequently used positive and negative MACS to enrich for PPE-like cells. Figure 2K shows robust immunocytochemical positivity for PPE markers SIX4 (a), EYA1 (a, c), and SIX1 (d) in PPE-like cells after LDN/SB/F/I treatment for 5 days. These PPE-like cells were also positive for SOX2, indicating expression of pro-sensory neuronal progenitors [4, 44]. Finally, RT-PCR analyses revealed that adding FGF2 reduced SOX10 expression (Supporting Information Fig. 1B), suggesting a PPE rather than a neural crest lineage. Semi-quantitative RT-PCR analyses revealed high levels of expression of $p75^{NTR}$ (Supporting Information Fig. 1).

Stage 2: PPE-Derived ONPs. Positive sorting for $p75^{NTR}$ and negatively sorting for TRA-1-81 (FACS) or TRA-1-60 (MACS) on D11 enriched the PPE-like cell population (Supporting Information Fig. 1E). With FACS, 21.5% ± 5.63% of hESC-derived PPE-like cells were TRA-1-81-negative and p75-positive ($n = 3$). Similarly, with MACS, 22.3% ± 7.67% of hESC-derived PPE-like cells were TRA-1-60-negative and p75-positive ($n = 3$), indicating that these two sorting methods were comparable for achieving desired purification. After purification, cells were differentiated into ONPs (Figs. 1. 3A).

Figure 3B demonstrates typical cell morphology after early- and mid-stage ONP treatment. Short but distinct neurite-like structures are visible. Immunocytochemistry revealed modest expression of ONP markers FOXG1 and GATA3 (Fig. 3C) at treatment day 5 and robust expression (Fig. 3D) of ONP markers PAX2, PAX8, SOX2, GATA3, and Nestin at treatment day 7 [4, 5, 40, 41, 45–48]. Quantification of Nestin-positive cells was performed at days 3, 7, and 10 (Fig. 3E) to evaluate ONP cell maturity. Nestin was highly expressed after treatment with W/F/I for 7 days (95.7% ± 1.76) compared with the N2B27-CDM-only control (14.7% ± 0.67%). However, even after 10 days of W/F/I treatment, one of SGN markers [9, 45, 49, 50] GATA3 was expressed in only 45.6% ± 4.41% of cells (Fig. 3F). Thus, while these cells expressed some ONP markers, they had not committed fully to auditory-specific lineages [51].

Exemplar and summary characterizations of late-stage ONPs are shown in Figure 4 for H1, H7, and H9 hESC lines. To obtain greater incidence of auditory-specific phenotypes, ONPs were treated with SHH, ATRA, EGF, and IGF-1 (S/R/E/F/I) (Figs. 1, 4A). Figure 4B shows GATA3 and FOXG1 immunocytochemistry after S/R/E/F/I treatment for 7 days. ONPs expressed β-III tubulin, a neuron-specific marker [52, 53] (Fig. 4C, first row). Cells also expressed NEUROD1 (a neuroblast marker [54]) and PAX8, but did not express E-cadherin (ECAD, an otic epithelial marker [40]) nor SOX10 (data not shown), suggesting that the cells differentiated toward an ONP lineage, rather than an otic epithelial lineage. Over 98% of cells were positive for GATA3 (98.3% ± 1.23% vs. 57.3% ± 3.85% without S/R/E/F/I treatment; $p < .05$, $n = 10$) and over 93 % of cells were positive for PAX8 (93.0% ± 3.05% vs. 59.6% ± 4.26% without S/R/E/F/I treatment; $p < .05$, $n = 10$). S/R/E/F/I treatment did not significantly change the proportions of cells positive for other ONP markers (e.g., FOXG1, Nestin, PAX2, and SOX2; Fig. 4D). Positivity for SOX2 and Nestin indicates that cells maintained ONP states and did not differentiate into neurons. The reproducibility of our differentiation protocol was evaluated at late-stage ONPs for H1, H7, and H9 hESC lines using immunocytochemical analyses on double-positive cells of PAX8 and GATA3 (Fig. 4E, 4F). Among those other ONP markers, PAX8, and GATA3 were chosen for this analysis, because S/R/E/F/I treatment resulted in uniquely greater protein expression in late-stage ONPs (Fig. 4D). Figure 4F shows comparable result on these three cell lines, which was consistent with other neuronal

Stem Cells Translational Medicine published by Wiley Periodicals, Inc. on behalf of AlphaMed Press

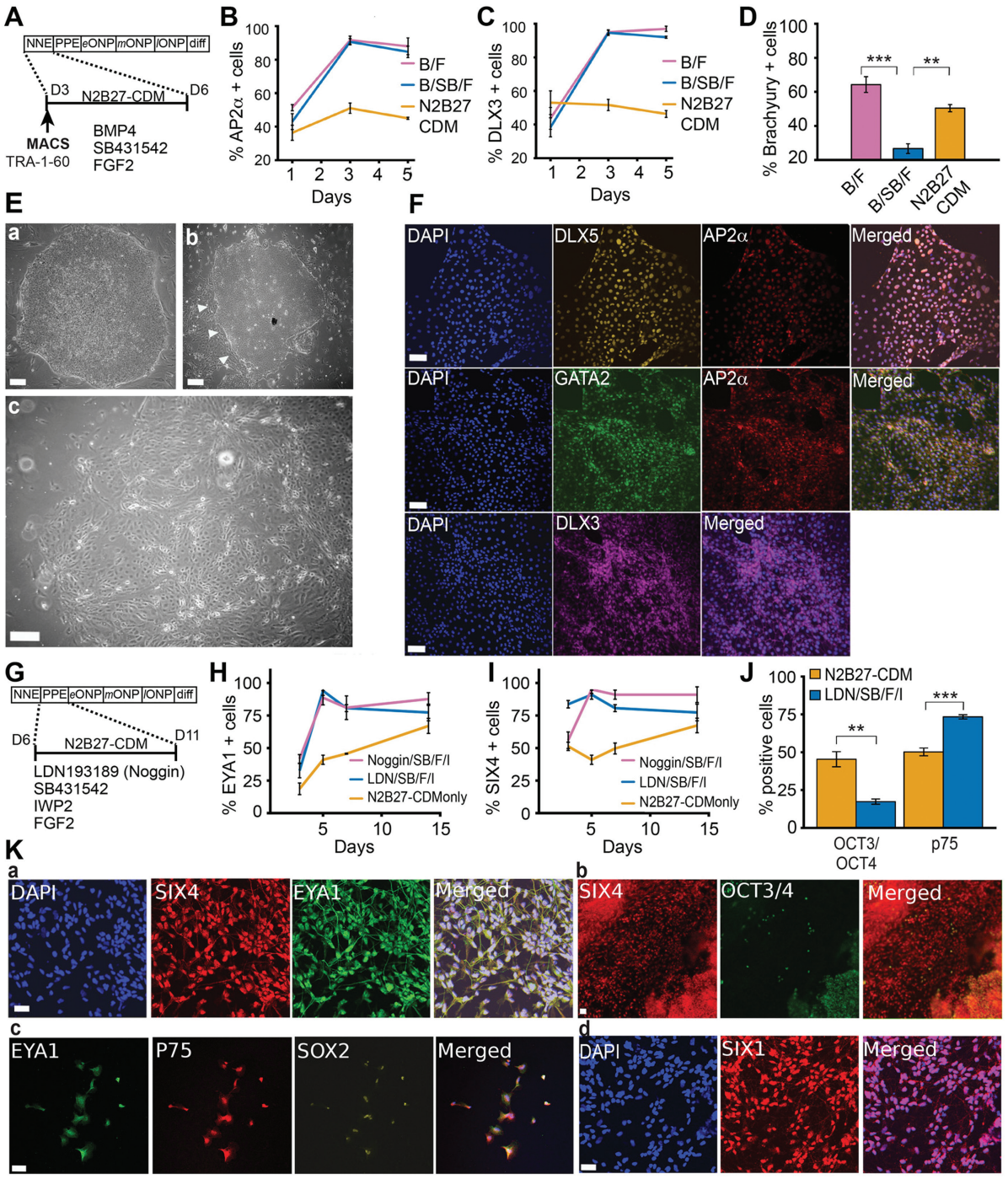

Figure 2. Assessment of induction of NNE-like **(A-F)** and PPE-like (**G-K**) cells. (A): Epoch and processing for NNE induction relative to the stepwise protocol (Fig.1). D: days. **(B, C)**: Quantification of AP2α- and DLX3-immunopositive cells ($n = 3$). Treatment with BMP4/FGF2 (B/F) or BMP4/SB431542/FGF2 (B/SB/F) for three days induced >90% of human embryonic stem cells (hESCs) to express AP2α and DLX3; the N2B27-CDM-only condition is shown for comparison. **(D)**: Quantification of Brachyury-immunopositive cells under three treatments: B/F, B/SB/F, and N2B27-CDM only ($n = 3$). Brachyury-positive cells were significantly reduced with B/SB/F (ANOVA, Tukey's post hoc test). **(E)**: Phase-contrast photomicrographs of (**Ea**) undifferentiated hESCs, **(Eb)** hESCs treated with B/SB/F for one day, and **(Ec)** hESCs treated with B/SB/F for three days. Scale bar: 100 μm. **(F)**: Immunocytochemistry fluorescence of B/SB/F treated hESCs for NNE markers DLX3, DLX5, AP2α, and GATA2. Scale bar: 100 μm. **(G)**: Epoch for PPE induction relative to the stepwise protocol. **(H, I)**: Quantification of EYA1- and SIX4-immunopositive cells ($n = 3$). Treatment with Noggin or LDN193189 induced significantly higher expression rates than N2B27-CDM alone at D5. **(J)**: Quantification of OCT3/4- and p75-positive cells ($n = 6$). The treatment with LDN193189 (or Noggin), SB431542, FGF2 and IWP-2 (labeled "LDN/SB/F/I") for 5 days significantly suppressed OCT3/4-positive cells relative to the N2B27-CDM control condition. Also, LDN/SB/F/I treatment significantly increased $p75^{NTR}$ positivity compared with N2B27-CDM (Student's *t* test). **(K)**: Immunocytochemistry of hESCs treated with LDN/SB/F/I for EYA1 **(Ka, Kc)**, SIX1/4 (Ka, Kb, **Kd**), OCT3/4 (Kb), p75 and SOX2 (Kc). Scale bar: 50 μm. **, $p < .01$; ***, $p < .001$. Abbreviations: B/F, BMP4/FGF2; B/SB/F, BMP4/SB431542/FGF2; BMP4: bone morphogenetic protein 4; DAPI, 4′,6-diamidino-2-phenylindole, dihydrochloride; FGF2: fibroblast growth factor 2; MACS: magnetic activated cell sorting; N2B27-CDM, chemically defined medium containing N2 and B27 supplements; NNE: nonneuronal ectoderm; ONP: otic neuronal progenitor; PPE: preplacodal ectoderm; TRA: trans retinoic acid.

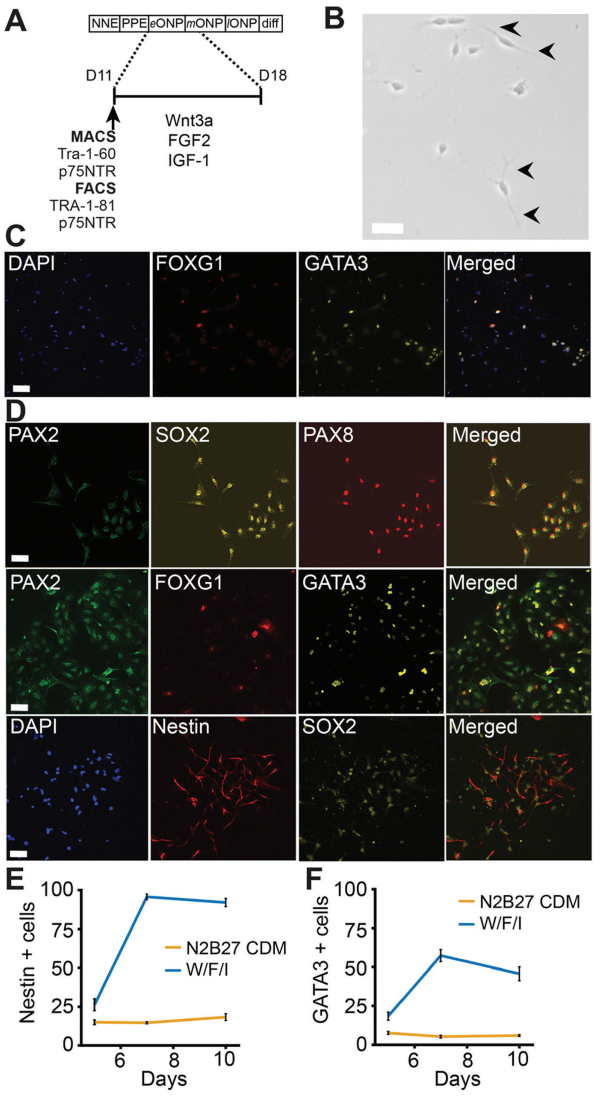

Figure 3. Assessment of induction of human embryonic stem cell (hESC)-derived early- and mid-stage ONPs. **(A)**: Indication of epoch and processing for early- and mid-stage ONP induction relative to the stepwise protocol of Figure 1. On day 11, hESC-derived PPE-like cells were dissociated into a single suspended state and then purified with FACS or MACS using $p75^{NTR}$ and TRA-1-81 antibodies. Treatment with Wnt3a, FGF2, and IGF-1 was started for 7 days. D: days. **(B)**: Phase-contrast photomicrograph of early-stage ONPs treated with Wnt3a, FGF2, and IGF2 in N2B27-CDM for 7 days. Note "neurite-like" processes radiating from the soma (black arrow). Scale bar: 50 μm. **(C)**: Immunocytochemistry of hESCs treated with Wnt3a, FGF2, and IGF-1 for 5 days shows modest expression of the ONP markers FOXG1 and GATA3. Scale bar: 100 μm. **(D)**: Immunocytochemistry fluorescence of hESCs treated with Wnt3a, FGF2, and IGF-1 for 7 days shows robust expression of the ONP markers PAX2, SOX2, PAX8, GATA3, and Nestin. Scale bar: 50 μm. **(E)**: Quantification of Nestin-positive cells with immunocytochemistry. Compared with N2B27-CDM, treatment with Wnt3a, FGF2, and IGF-1 (labeled "W/F/I" in figure) increased Nestin expression rate. **(F)**: Quantification of GATA3-immunopositive cells. Treatment with Wnt3a, FGF2, and IGF-1 (labeled "W/F/I") also increased the GATA3 expression rate when compared with the N2B27-CDM control condition. Expression rate peaked at 7 days, and further treatment did not increase GATA3. Abbreviations: DAPI, 4′,6-diamidino-2-phenylindole, dihydrochloride; FACS: fluorescence activated cell sorting; FGF2: fibroblast growth factor 2; IGF-1: insulin-like growth factor 1; MACS: magnetic activated cell sorting; N2B27-CDM, chemically defined medium containing N2 and B27 supplements; NNE: nonneuronal ectoderm; ONP: otic neuronal progenitor; PPE: preplacodal ectoderm.

differentiation protocol mainly using H1, H7, and H9 cell lines [27, 55–61].

Figure 4G summarizes RT-PCR analyses during the sequential step-wise treatments to further characterize the ONPs. W/F/I treatment combined with S/R/E/F/I treatment at the late-ONP stage resulted in the loss of PAX6 (a marker for neuroectoderm [62] and lens and nasal placode [17]) and PAX3 (a marker for the trigeminal placode [17]). PAX2 (a marker for otic and epibranchial placodes [17]) was stably expressed until late ONP stage. PAX8 (a marker for the otic and epibranchial placodes [17]) was only weakly expressed in the NNE stage. HOXB1 and HOXB2 were expressed until the NNE stage, whereas HOXA2 and HOXB4 were stably expressed until the late-ONP stage. Finally, SALL4 was strongly expressed until the PPE stage and gradually declined as otic neuronal differentiation progressed.

Stage 3: ONP-Derived SGN-Like Cells. We next sought to determine the capacity of enriched late-stage ONPs to differentiate into mature neurons. We initiated differentiation by removing mitogens (FGF2, EGF, and SHH) and adding factors that support SGN survival, including BDNF [63, 64], NT-3 [63, 65], and IGF-1 [66, 67]. Figure 5B indicates typical morphology of late-stage ONPs treated for 4 weeks with the strategy shown in Figure 4A. Cells displayed bipolar morphology typical of SGNs, with two long neurites extending bilaterally from the soma (white arrows). Figure 5C shows immunocytochemistry of late-stage ONPs differentiated into SGN-like cells for 3-6 weeks using H1, H7, and H9 hESC lines. After treatment for one week, ONPs no longer expressed precursor markers Nestin, SOX2, or SOX10 (data not shown). By 2-4 weeks, cells were positive for peripheral nervous system (PNS) sensory neuron marker peripherin and BRN3A [4, 68] and neuronal marker β-III tubulin and MAP2 [58]. Cells were also positive for TrkB and TrkC receptors, characteristic of human SGNs [63], and for GluA2-4 and Vglut1, 2, and 3, characteristic of glutamatergic neurons [4, 69]. Cells were no longer positive for Ki67, indicating exit from the cell cycle. These observations indicate that the cells were appropriately differentiated toward the SGN phenotype. However, scattered cells expressed glial markers vimentin and glial fibrillary acidic protein, indicating that cultures were not pure for human SGN characteristics. As illustrated in Figure 5C, virtually all SGN-like cells were positive for vasoactive intestinal polypeptide (VIP) and neuropeptide Y (NPY) and negative for substance P. The cells were also positive for Pejvakin (PJVK) protein [70] and transmembrane protease serine 3 (TMPRSS3) [71].

Figure 5D summarizes the expression of a number of other traits in the SGN-like cells compared with control cells treated only with NIM for 4 weeks. We enumerate the following %-positive cell measures: neurotrophic factors: TrkC–SGN: 98.7 ± 1.33, Control: 2.3 ± 1.2, $p < .001$; TrkB–SGN: 95.7 ± 3.3, Control: 4.3 ± 1.5, $p < .001$; glutamatergic neuronal markers: Vglut1–SGN: 93.0 ± 3.2, Control: 53.0 ± 6.1, $p < .05$; GluA2-4–SGN: 98.0 ± 1.2, Control: 75.0 ± 4.9, $p < .05$; PNS sensory markers peripherin–SGN: 82.7 ± 2.9, Control: 13.6 ± 1.0, $p < .01$; and Brn3a–SGN: 46.0 ± 1.2, Control: 6.3 ± 2.0, $p < .05$).

To assess background staining or staining nonspecific to primary antibodies, samples were treated identically to experimental immunocytochemistry conditions using secondary antibodies with the omission of primary antibody during overnight incubation. Negative results obtained from these

Stem Cells Translational Medicine published by Wiley Periodicals, Inc. on behalf of AlphaMed Press

secondary-antibody-only controls are shown in Supporting Information Figure 4.

Physiological Assessments of hESC-Derived SGN-Like Cells

Electrophysiological assays examined the functionality and characteristics of hESC-derived SGN-like cells. By adding high-concentration (50 mM) KCl into solution, calcium imaging with Fura-2 dye (Fig. 6A) showed transient calcium influx upon depolarization, indicating responsive voltage-gated calcium channels. Voltage-clamp recordings [Fig. 6B(a-b)] showed transient depolarizing inward currents and subsequent hyperpolarizing outward currents. The current-voltage function of Fig. 6B(c) demonstrates transmembrane conductance and threshold for regenerative current near −20 mV. Whole-cell current clamping also showed that injected depolarizing currents induced action potentials [Fig. 6B(d)].

We also obtained measurements from naïve mouse SGNs at P2-P3 for control comparisons. Matching data sets were obtained from three mouse SGNs at P2-P3 with representative response curves shown in Figure 6C(a-d). For the control SGNs, inward and outward currents were triggered under voltage clamp [Fig. 6C(a-b)], but with lower thresholds, larger membrane currents [Fig. 6C(c)], and larger spike amplitudes (C-d). Comparisons with these control data are summarized in Figure 6D(a-c) and show that the SGN-like cells had immature response characteristics. First-spike latency for the SGN-like cell was at least twice as great as those from the three control SGNs [Fig. 6 D(a)] and spike widths from the hESC-derived cell were longer (Fig. 6D(a), $p < .0001$). Transmembrane currents were an order of magnitude lower for the hESC-derived cell [Fig. 6D(b)], which also required larger command voltages for action-potential initiation. Spike amplitudes [Fig. 6D(c)] were in all cases smaller than those of controls ($p < .0001$).

Survival, Migration, and Differentiation of hESC-Derived SGN-Like Cells in Coculture With Auditory Brainstem

We also examined cocultures of hESC-derived late-stage ONPs and rat auditory brainstems containing the CN (Supporting

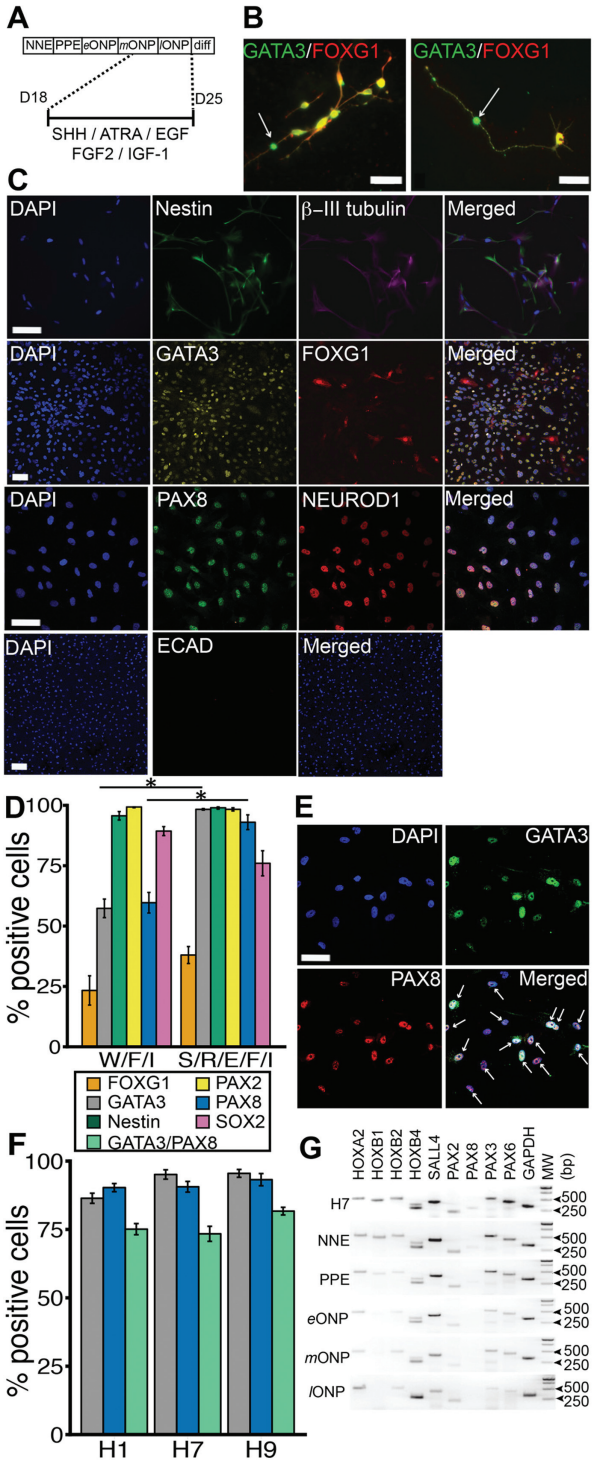

Figure 4. Assessment of induction of late-stage ONPs using H1, H7, and H9 human embryonic stem cells (hESC) lines. **(A)**: Indication of epoch and processing for late-stage ONP induction relative to the stepwise protocol of Figure 1. On day 18, seven-day treatment with SHH, ATRA, EGF, FGF2, and IGF-1 was initiated. **(B)**: Morphology of hESC-derived late-stage ONPs. Some ONPs (white arrows) extend long neurite-like structures **(C)**: Immunocytochemistry of hESCs from the three cell lines, treated with SHH, ATRA, EGF, FGF2, and IGF-1 treated for 5 days show expression of the ONP markers Nestin, GATA3, and FOXG1. β-III tubulin, PAX8, and NEUROD1 were also expressed. Staining for ECAD was negative (white arrow indicates that only one cell was expressed ECAD in this particular field). Scale bar: 100 μm. **(D)**: Quantification of late-stage ONP markers based on immunocytochemistry. Expression of GATA3 and PAX8 was significantly higher with additional treatment of SHH, ATRA, EGF, FGF2, and IGF-1 ("S/R/E/F/I") compared with Wnt3a, FGF2, and IGF-1 ("W/F/I") treatment alone (one-way ANOVA with Tukey's post hoc test: *, $p < .05$). **(E)**: Exemplary H1-hESC immunocytochemical imagings of late-stage ONPs with GATA3 and PAX8. In merged image, arrows indicate cells achieving threshold expression for quantitation. Scale bar: 50 μm. **(F)**: Quantitative analysis of GATA3 and PAX8 double-positive cells in H1, H7, and H9 hESC line-derived late-stage ONPs. There were no statistically significant differences among these three hESC-lines, $p > .05$, One-way ANOVA. **(G)**: RT-PCR analysis for *HOX* genes (*HOXA2, HOXB1, HOXB2, HOXB4*), *PAX* genes (*PAX2, PAX3, PAX6, PAX8*), *SALL4*, and a housekeeping gene (*GAPDH*) performed at five different stages of otic differentiation; H7 (undifferentiated stage), NNE, PPE, early-stage ONPs (*e*ONP), mid-stage ONPs (*m*ONP), and late-stage ONPs (*l*ONP) as defined in Figure 1. MW: molecular weight in base pairs. Abbreviations: DAPI, 4′,6-diamidino-2-phenylindole, dihydrochloride; ECAD, E-cadherin; FGF2: fibroblast growth factor 2; IGF-1: insulin-like growth factor 1; NNE: nonneuronal ectoderm; PPE: preplacodal ectoderm; ONP: otic neuronal progenitor; SHH: Sonic Hedgehog; ATRA: all-trans retinoic acid;

Information Fig. 2A-2D). Figure 7 summarizes neurite growth for CN cocultures [Fig. 7A(a-d, e-h)] or NST coculture [Fig. 7B(a-c)]. At day 28, transplanted ONPs, originally placed 750 μm from the CN, had migrated toward the CN {white arrow in [Fig. 7(a) and (e)]}. Figure 7A(c, enlarged in d) shows that some ONPs (expressing peripherin, two white triangles) extended neurites to the surrounding transplanted cells as well as to the CN. Additionally, synaptophysin-positive puncta were observed, suggesting synaptic connections to the ONP aggregates [white arrows, Figure 7A(d, h). Some transplanted ONPs were positive for BRN3A, suggesting PNS sensory neuronal differentiation in the coculture (Supporting Information Fig. 2F]. Representative photomicrographs of hESC-derived ONPs cocultured with the NST are shown in Fig. 7B. The direction of migration of the ONPs is again shown by white arrows in Figure 7B(a). Although hESC-derived ONPs extended some neurites to the NST [white arrowhead, Fig. 7B(c)], they also extended neurites to adjacent brainstem areas (white arrows). There were no significant differences in the numbers of BRN3A-positive and peripherin-positive cells in the cocultures; however, significantly more synaptophysin-positive ONPs were present in cocultures with the CN than with the NST (Fig. 7C; CN: synaptophysin 97.7% ± 0.6% vs. NST: synaptophysin 38.8% ± 3.0%, Student's *t* test: $p < .001$). Furthermore, the cells extended more neurites to the CN than to the NST (Fig. 7D; CN: 14.2 ± 0.94, NST: 2.33 ± 0.49, Student's *t* test: $p < .001$).

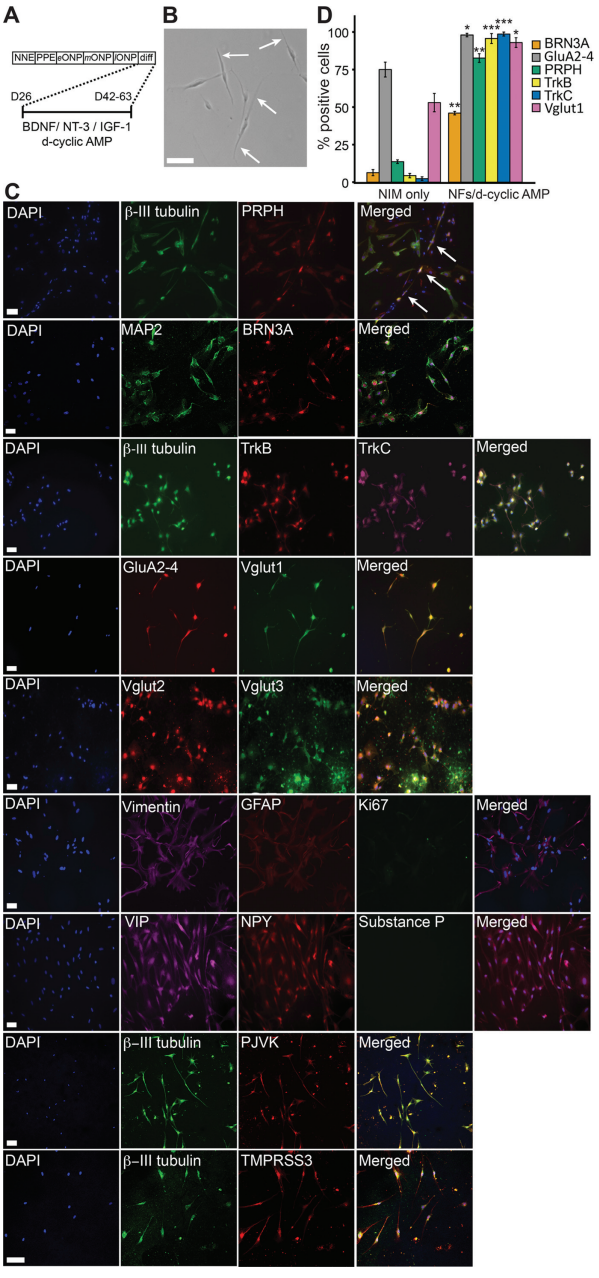

Physiological Assessment of hESC-Derived ONPs in an Organotypic Rat Brainstem Coculture

VSD activity (see Supporting Information) was evoked by electric stimulation of the coculture, shown in Figure 7E(a-b). VSD fluorescence was evident from SGN-like cells located between the IKVAV gel region and brainstem, consistent with aforementioned ONP migration toward the CN. Activity occurred at cell resting states [Fig. 7F(a)], consistent with normally hyperpolarized neuronal cells. Twenty-nine regions of interest (ROIs) were identified and plotted [red circles in Fig. 7F(b)] over the same image, then level-adjusted to reduce background noise (adjusted for visualization purpose only). The mean ROI diameter was 18.5 μm, within human and research-animal SGN diameters (see Supporting Information). Cells were stimulated by 25 μA 100 μs cathodic pulses. Figure 7F(c) shows the electrically-evoked VSD response, obtained by subtracting the resting-state image from that obtained with electrical stimulation; lighter patches aligned with the ROIs indicate evoked depolarization. The null hypothesis that electrically evoked activity caused no VSD intensity change was rejected ($p < .05$) for 24 of 29 ROIs, with *p* values shown by color-filled circles in Figure 7F(d), adjusted for false discovery [72]. Additional information is included in the Supporting Information.

Figure 5. Assessment of induction of spiral ganglion neuron (SGN)-like glutamatergic neurons from late-stage ONPs derived from H1, H7, and H9 human embryonic stem cell (hESC) lines. **(A)**: Stepwise treatment strategy for SGN induction. On day 26, treatment with BDNF, NT-3, IGF-1, and db-cyclic AMP was started in NIM for 14-21 days. D: days. **(B)**: Phase-contrast micrograph of SGN-like cells after 21 days of neuronal induction. Note the bipolar nature of the cells (arrows indicate bipolar processes). **(C)**: Immunocytochemistry of hESCs treated with BDNF, NT-3, IGF-1, and db-cyclic AMP in NIM shows expression of a neuronal marker (β-III tubulin), peripheral neuronal markers (PRPH and BRN3A), tyrosine kinase receptors (TrkB, TrkC), Vglut1, Vglut2 and Vglut3, an AMPA receptor (GluA2-4), vimentin, GFAP, neuropeptides (VIP and NPY), PJVK, and TMPRSS3. Scale bars: 50 μm. **(D)**: Quantification of marker expression based on immunocytochemistry in hESCs treated with BDNF, NT-3, IGF-1, and db-cyclic AMP. (labeled with "NFs/db-cyclic AMP"). Compared with those treated only with N2B27-CDM, GluA2-4, Vglut1 ($p < .05$), BRN3A, PRPH ($p < .01$), TrkB, and TrkC ($p < .001$) expression rates were statistically significantly higher in treated cells, using one-way ANOVA with Tukey's post hoc test: *, $p < .05$; **, $p < .01$; ***, $p < .001$. Abbreviations: BDNF, human brain-derived neurotrophic factor; DAPI, 4′,6-diamidino-2-phenylindole, dihydrochloride; d-cyclic AMP, dibutyryl-cyclic AMP GFAP, glial fibrillary acidic protein; NT-3, human neurotrophin-3; IGF-1, insulin-like growth factor 1; NIM, neuronal induction medium; NNE: nonneuronal ectoderm; NPY, neuropeptide Y; ONP: otic neuronal progenitor; PJVK, Pejvakin, PPE: preplacodal ectoderm; PRPH peripherin; TMPRSS3, transmembrane protease serine 3 VIP, vasoactive intestinal polypeptide; Vglut1, Vglut2 and Vglut3, vesicular glutamate transporters.

Stem Cells Translational Medicine published by Wiley Periodicals, Inc. on behalf of AlphaMed Press

Discussion

The ability to generate SGNs from stem cells is required to realize clinical cell-replacement therapies for SNHL. We developed a protocol for reliably and reproducibly deriving purified populations of ONPs and SGN-like cells from hESCs. Chen et al. [5] and Needham et al. [44] previously reported that SGN-like cells can be generated from hESCs. Our work extends these findings by adopting a stepwise protocol closely based upon known developmental stages of the normal ear. We showed that these SGN-like cells express appropriate markers, preferentially extend neurites to the CN rather than to unrelated nuclei, and can generate action potentials, though with immature characteristics. This work advances our understanding of SGN development and developing stem cell therapy for SNHL.

SGNs rely primarily on glutamate to transmit sensory information to the CNS [73]. Our protocol successfully generated glutamatergic SGN-like cells (>98% expressing Glut1 and GluA2-4). Furthermore, nearly all hESC-derived SGNs expressed TrkB and TrkC neurotrophin receptors, which respond to BDNF and NT3, respectively [63]. VIP and NPY were expressed by the SGN-like cells, a characteristic of adult type I or II SGNs [74]. A varying degree of positive staining pattern of substance P on adult human SGNs was previously observed [74], consistent with our results. Our hESC-derived SGN-like cells expressed PJVK protein, hypothesized to underlie auditory neuropathic hearing losses associated with SGN-specific loss [75]. Recently, this protein was found in human SGNs although expression of this protein is not specific to human SGNs [75]. Furthermore, type-II transmembrane serine protease (TMPRSS3), found in SGN cell bodies [76, 77], were also expressed by our cells, although once again its presence is not specific to human SGNs.

Importantly, the pattern of transcription factor expression by our cells is similar to the human SGN lineage. A zinc finger transcription factor of the spalt gene family, Sally 4, is expressed in the otic placode [78]. SALL4 was also strongly expressed until the PPE stage, as shown by RT-PCR, suggesting that our hESC-derived ONPs were of otic placode lineage. The *Hox* genes, coding for a large family of homeobox-containing proteins, display rhombomere-restricted expression patterns and provide early

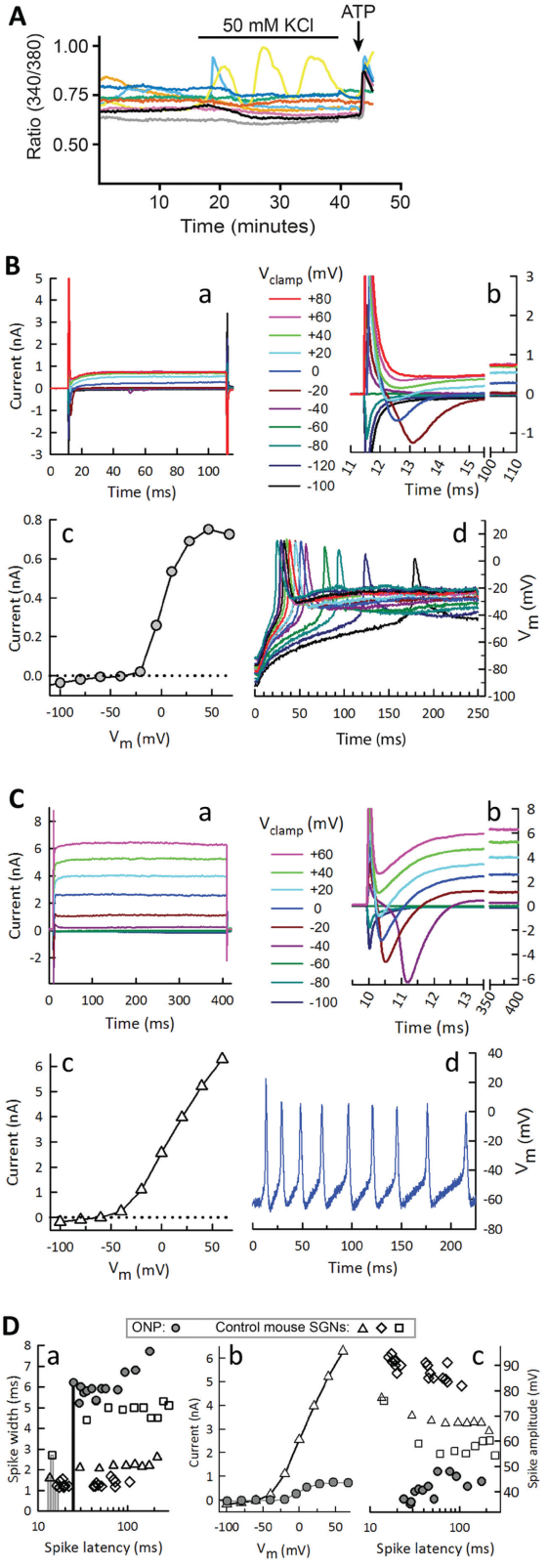

Figure 6. Electrophysiological responses and properties of SGN-like cells and neonatal mouse SGNs. In **(A)** and **(B)**, human embryonic stem cell (hESC)-derived ONPs were treated with human brain-derived neurotrophic factor, human neurotrophin-3, insulin-like growth factor, and dibutyryl-cyclic AMP for 21 days. (A): Calcium imaging with Fura-2 showed calcium transients evoked by depolarization with 50 mM KCl, with the epoch of KCl application shown by the horizontal bar. ATP (10 μM) was added as a control for metabolically active neurons. **(B): (Ba)** Whole-cell voltage-clamp recordings of SGN-like cell subjected to 100 ms rectangular voltage pulses at the potentials indicated. Transient depolarizing inward currents followed by hyperpolarizing outward currents were evident for command voltages > -40 mV, with **(Bb)** showing the first 16 ms of the response shown in (Ba). Steady-state current levels (averaged over the 75-120 ms epoch) are plotted vs. clamped potentials to demonstrate membrane transconductance **(Bc)**; range of strong current influx is initiated at about -20 mV. In **(Bd)**, whole-cell current-clamp recordings of the SGN-like cells shows action potential initiation. In **(C)**, comparable data sets (corresponding to those in A) are shown from normal mouse SGNs. Key differences between our hESC-derived cells and normal mouse SGNs are highlighted in **(D)**, with data from hESC-derived cells shown by filled circles. Spike widths and first-spike latencies (vertical bars) were both prolonged in the hESC-derived cells **(Da)**. Threshold of action-potential activation and maximum transmembrane currents were higher and lower, (respectively), for the hESC cells **(Db)** and spike amplitudes were lower **(Dc)** relative to the normal mouse SGN values. Abbreviations: ONP: otic neuronal progenitor; SGN, spiral ganglion neuron.

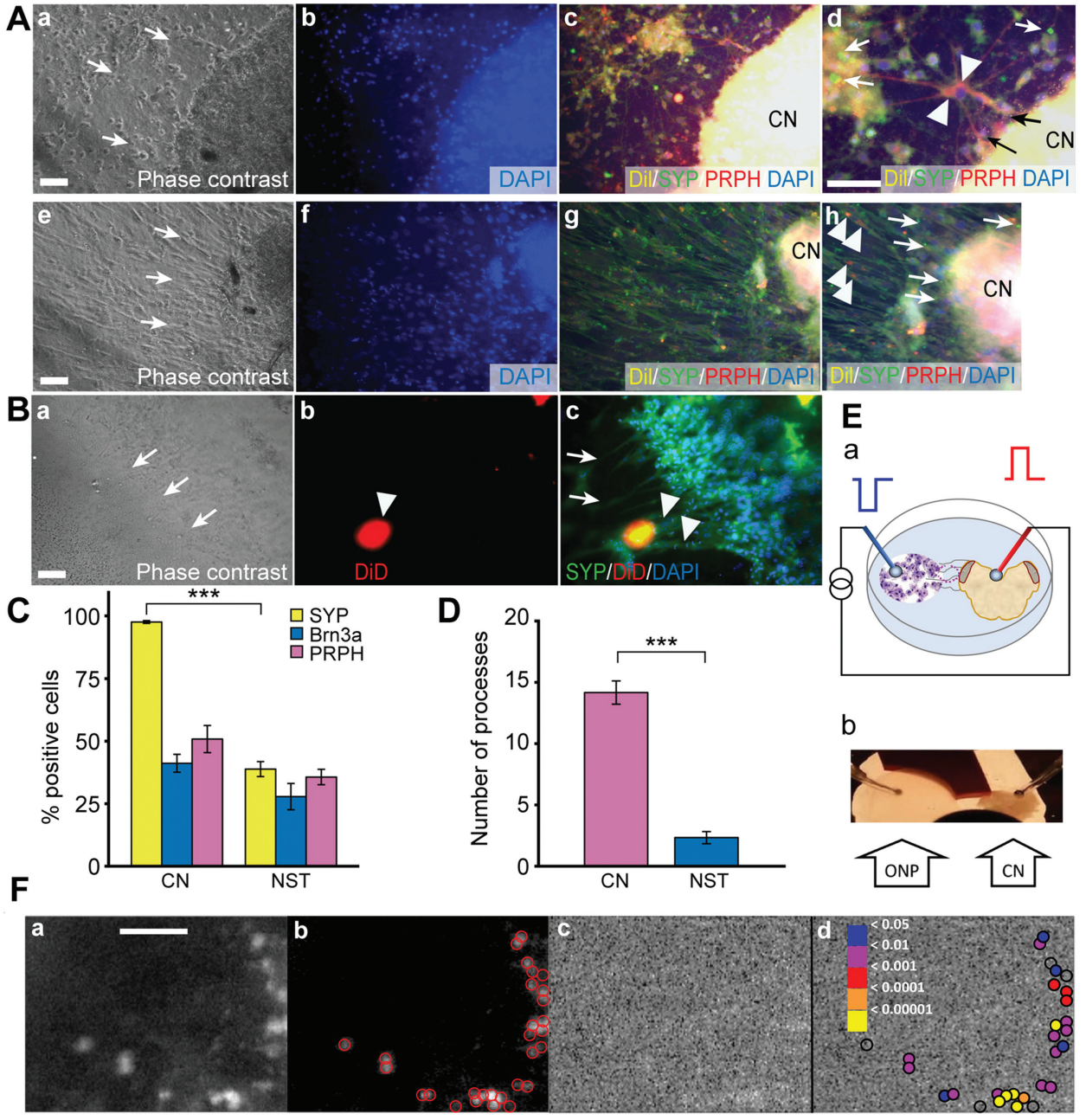

Figure 7. Analyses of spiral ganglion neurons/brainstem co-cultures. **(A)**: otic neuronal progenitor (ONP) cocultures with brainstem containing CN at P13. **(Aa-Ad)** and **(Ae-Ah)** present two representative data sets from two cultures. **(Aa, Ae)**: Phase-contrast shows ONPs placed 750 μm away from the CN migrated toward the CN (arrows indicate migration). **(Ab, Af)**: DAPI. **(Ac, Ad, Ag, Ah)**: Immunocytochemistry. ONPs were positive for peripherin (white triangular arrows in (Ad, Ah)) and extended neurites (black arrows, (Ad)) to the DiI-labeled CN. Synaptic puncta (white arrows, (**A**d, Ah)) are positively stained for synaptophysin. **(B)**: Coculture with brainstem containing NST at P14. **(Ba)**: Phase-contrast (white arrows: migration vector), **(Bb)**: DiD-labeled NST (arrowhead), **(Bc)**: Immunohistochemistry. DiD (red/orange) indicates NST. **(C)**: Quantification of immunohistochemistry for synaptophysin, BRN3A, and peripherin ($n = 4$). **(D)**: Quantification of number of neurite-like processes extending to CN or NST ($n = 4$). ***, $p < .001$ (Student's t test). **(E): (Ea)**: Diagram of electrically stimulated coculture. Cathodic (blue) electrode positioned within ONP aggregate; anodic (red) electrode in brainstem medial to CN. **(Eb)**: Photograph showing electrodes, ONPs, and CN. **(F)**: Physiologic assessment of ONPs using VSD. **(Fa)**: Bright regions indicate depolarized cells at resting-state. **(Fb)**: Image of (Fa) thresholded prior to selecting regions of interest (red circles). **(Fc)**: Image showing difference between electrically evoked and resting-state fluorescence, revealing faint electrically evoked excitation regions. **(Fd)**: Statistical analysis of ROIs; 24 of 29 were significance ($p < .05$). All scale bars: 100 μm. Abbreviations: CN, cochlear nucleus; DAPI, 4′,6-diamidino-2-phenylindole, dihydrochloride; NST, nucleus of solitary tract; SYP: synaptophysin, PRPH: peripherin.

patterning information to progenitors [79]. In turn, the expression of several specific *Hox* genes is maintained through later stages of circuit formation in distinct, rhombomere-derived neuronal subpopulations of the hindbrain sensory nuclei, including the CN [79]. *Hox*b1 in the hindbrain is required in the facial motor nucleus and the primitive peripheral facial nerve for proper connectivity [80]. Our RT-PCR results indicated that, as differentiation progressed to more mature ONP stages, the treatment induced the expression

Stem Cells Translational Medicine published by Wiley Periodicals, Inc. on behalf of AlphaMed Press

of *HOXA2*, *HOXB2,* and *HOXB4* and suppressed *HOXB1*. As shown by mouse in situ hybridization, *Hoxa2* is highly expressed in the ventral portion of the CN (VCN), the first main ascending relay point of SGNs in the auditory system, until postnatal developmental stages [81]. Similarly, *Hoxb2* transcripts are found in newborns in the main hindbrain relay nuclei of the auditory circuit, such as the VCN [81]. By contrast, *Hoxb1* null mutants exhibit distinct developmental defects on the developing facial nerve originating from the r4 domain of the developing hindbrain [82]. Collectively, these studies indicate that our cells expressed the appropriate *Hox* genes for the otic lineage.

Our RT-PCR results demonstrating the loss of PAX6 (a marker for the lens and olfactory placode) and PAX3 (a marker for the trigeminal placode) along with persistent expression of PAX2 (a marker for the otic and epibranchial placodes) also indicate that late-stage ONPs had appropriate regional specification. Developmentally, all cranial placodes express *Pax* genes shortly after PPE induction, with the most rostral (nose and lens) expressing *Pax6*, the intermediate level (trigeminal) expressing *Pax3,* and most caudal (ear and epibranchial) expressing *Pax2* [42]. This indicates that peripheral neurons derived from late-stage ONPs were guided specifically to otic lineages. Induction of *HOXB4* in the late-ONP stage (shown by RT-PCR) also suggests that the late-stage ONPs were appropriately regionally specified (i.e., r6/r7), as *Hoxb4* is maintained at the r6/r7 boundary in the mouse embryo [83]. Although hESC-derived ONPs preferentially extended neurites to the CN in our cocultures, some ONPs migrated toward, and appeared to extend neurites to, the NST. Along with our RT-PCR results, this suggests that our ONPs may have included cells of the epibranchial as well as the otic lineage. Nevertheless, both the number of neurites extending to the CN and the number of synaptophysin-positive cells in CN cocultures were significantly higher than those extending to the NST in cultures containing CN and NST targets.

Because there is no single specific ONP molecular marker, we used GATA3 as an indicator to measure ONP maturity. Previous studies indicated that Trans-acting T cell specific transcription factor GATA-3 is a likely regulator of early SGN development. Consistent with this notion, *Gata3* was expressed in mouse and chick SGNs but not in vestibular ganglions [46, 84]. Of late-stage ONPs, 98.3% were positive for GATA3 via immunocytochemistry, indicating that the S/R/E treatment effectively increased GATA3 positivity on ONPs. Notably, our hESC-derived late-stage ONPs were also predominantly positive for PAX2, PAX8, SOX2, GATA3, NEUROG1, and NEUROD1, but negative for ECAD. These finding suggest that our ESC-derived late-stage ONPs were in fact ONPs rather than otic vesticle epithelial progenitors.

Interestingly, the rate of BRN3A expression in our hESC-derived cells that differentiated to late-stage ONPs was only 46% compared with 82.7% expression of peripherin, another PNS sensory marker. This is consistent with a previous finding using SHH/RA to induce PNS sensory neurons from MSCs [26]. A study using human fetal inner-ear stem cells indicated that only SHH and FGF2 are required to induce *BRN3A* expression [50] and noted that the combination of IGF-1 and FGF2 appeared to prevent neuronal differentiation by reducing *BRN3A* expression. Thus, our treatment for generating late-stage ONPs, which contained SHH, ATRA, EGF, and IGF-1, might not have been optimal for generating both ONPs and SGN-like neurons. Our finding that IGF-1 helped to support neuronal differentiation of ONPs is surprising, given previous reports of its effect in rat, mouse, and chick [21, 22, 85]. This emphasizes the importance of studying human system.

Our study used diffusible-ligand treatments to derive SGN-like cells. Such treatments typically have narrow spatial and temporal response windows, which may pose practical problems and compromise across-laboratory reproducibility [27]. An alternative is to generate SGNs through nucleofection of appropriate transfection factors. However, our initial yields using double nucleofection with PAX2 and PAX8 were extremely low (data not shown).

Though not our study's focus, we showed physiological measures consistent with biophysically active neurons using calcium imaging, whole-cell clamping, and VSD. Our whole-cell voltage-clamp data suggest that SGN-like cells are immature in terms of temporal properties, currents, and spike amplitudes, possibly linked to sub-adult numbers of ion channels and myelination. Needham et al. (2014) assessed several electrophysiologic properties of their hESC-derived SGN-like cells and found similar abnormalities in slower kinetics, small amplitudes, and smaller ionics currents, consistent with the immature responses we observed. Wider and lower-amplitude action potentials, longer latencies, and smaller ionic currents would predict abnormal auditory brainstem response (ABR) latencies, thresholds, and amplitudes, contrasting with the near-normal ABRs from gerbils treated with hESCs [5]. Clearly, more physiological studies are needed to resolve these differences. Ectopic placement of hESC-derived SGN-like cells [5] may be expected to result in abnormal response growth and altered representation of the exquisite frequency tuning of the cochlea. The popular remedy of cochlear implantation requires a good understanding of electrically-evoked SGN properties and tonotopic representation. Next-generation cochlear prostheses may develop into an adjunct therapy to stem-cell implantation. Thus, better knowledge of acoustically and electrically evoked responses will be needed for translating results to clinical practice.

Conclusion

We developed a refined stepwise generation of functional hESC-derived SGN-like cells with appropriate expression of most markers found in normal, developing SGNs. Treatment of hESCs with human orthologs of ligands, small molecules, and neurotrophic factors present in chick, *Xenopus* and murine inner ear embryogenesis generated a relatively pure population of cells phenotypically similar to SGNs that were functionally active and preferentially made synaptic connections to the CN. The ability to selectively control differentiation of hESCs into SGN-like cells is significant for (a) understanding the mechanisms regulating human SGN lineage commitment, (b) development of cell-replacement therapy for profound SNHL, and (c) high-throughput screening for agents that promote SGN survival.

Acknowledgments

We thank Dr. Moses V. Chao at New York University for kindly providing us with his $p75^{NTR}$ antibody; Paul Mehl and Jeffrey Nelson at Northwestern University Flow Cytometry Core Facility; Evangelos Kiskinis, M.D. at Northwestern University Stem Cell Core Facility; Wensheng Liu, M.D. at Northwestern University Imaging Core Facility; Dr. Omotara Mariam Sulman (University of Minnesota), and Dr. Chris Gouveia (NU) for assistance

with rat brainstem coculture; and Himanshi Desai for assistance with confocal microscopy. Special thanks are given to Drs. Eric J. Berns (NU), Nicholas Stephanopoulos (Arizona State University), and Zaida Alvarez Pinto (NU) for the provision of the IKVAV-PA gel; Dr. Evan W. Miller (University of California Berkeley) for insightful suggestions on VSD; Dr. Chian-Yu Peng (NU) for PCR analysis on *HOX* genes; Dr. Karl R. Koehler (Indiana University) for suggestion on antibody of PAX8 for immunocytochemistry; Dr. Steven T. Kosak (NU) for help in hESC (WAH9) culture; Dr.Vasil Garat (NU) for help in hESC (WAH1) culture, and Dr. Anil Wadhwani for proofreading. This work was supported by the American Otological Society Clinician Scientist Award (AJM), the Triological Society/American College of Surgeons Clinician Scientist Award (AJM), the Department of Otolaryngology of Northwestern University, an NIH K08 Clinician Scientist Award K08DC13829-02 (AJM), The office of Naval Research # N00014-12-1-0173 (DSW), and an NIH P30 NS081774 (JAK). Finally, A.J.M. acknowledges the support and encouragement of his late father, Tetsuo Joseph Matsuoka, M.D., D.M.Sc.

Author Contributions

A.J.M.: conception and design, financial support, collection and/or assembly of data, data analysis and interpretation, manuscript writing, final approval of manuscript; Z.M., K.H., A.B., C.A.M., D.M.C.., and S.K.: collection and/or assembly of data, data analysis and interpretation, manuscript writing; C.Z. and M.T.-M.: collection and/or assembly of data; A.N.E.: provision of study material or patients, manuscript writing; D.S.W.: provision of study material or patients, Collection and/or assembly of data; L.L. and T.M.: administrative support; S.I.S.: provision of study material, final approval of manuscript; J.A.K: conception and design, manuscript writing, financial support, provision of study material or patients, data analysis and interpretation, final approval of manuscript.

Disclosure of Potential Conflicts of Interest

The authors indicate no potential conflicts of interest.

References

1 World Health Organization. Deafness and hearing loss (Fact sheet N°300). 2015. Available at http://www.who.int/mediacentre/factsheets/fs300/en/. Accessed November 11, 2016.

2 Shi F, Corrales CE, Liberman MC et al. BMP4 induction of sensory neurons from human embryonic stem cells and reinnervation of sensory epithelium. Eur J Neurosci 2007;26:3016–3023.

3 Corrales C, Pan L, Li H et al. Engraftment and differentiation of embryonic stem cell–derived neural progenitor cells in the cochlear nerve trunk: Growth of processes into the organ of corti. J Neurobiol 2006;66:489–500.

4 Gunewardene N, Bergen N Van, Crombie D et al. Directing human induced pluripotent stem cells into a neurosensory lineage for auditory neuron replacement. Biores Open Access 2014;3:162–175.

5 Chen W, Jongkamonwiwat N, Abbas L et al. Restoration of auditory evoked responses by human ES-cell-derived otic progenitors. Nature 2012;490:278–282.

6 Koehler KR, Alexander KM, Hashino E. Recapitulating inner ear development with pluripotent stem cells: Biology and transition. In: Raymond R, Varela-Nieto I, eds. Development of Auditory and Vestibular Systems. 1st ed. Amsterdam: Elsevier, 2014:213–247.

7 Rubel EW, Fritzsch B. Auditory system development: Primary auditory neurons and their targets. Annu Rev Neurosci 2002;25:51–101.

8 Chambers SM, Fasano CA, Papapetrou EP et al. Highly efficient neural conversion of human ES and iPS cells by dual inhibition of SMAD signaling. Nat Biotechnol 2009;27:275–280.

9 Koehler KR, Mikosz AM, Molosh AI et al. Generation of inner ear sensory epithelia from pluripotent stem cells in 3D culture. Nature 2013;500:217–221.

10 Wilson P, Hemmati-Brivanlou A. Induction of epidermis and inhibition of neural fate by Bmp-4. Nature 1995;376:331–333.

11 Wilson P, Lagna G, Suzuki A et al. Concentration-dependent patterning of the Xenopus ectoderm by BMP4 and its signal transducer Smad1. Development 1997;124:3177–3184.

12 Kwon H-J, Bhat N, Sweet EM et al. Identification of early requirements for preplacodal ectoderm and sensory organ development. PLoS Genet 2010;6:1–14.

13 Koehler KR, Hashino E. 3D mouse embryonic stem cell culture for generating inner ear organoids. Nat Protoc 2014;9:1229–1244.

14 Leung AW, Kent Morest D, Li JYH. Differential BMP signaling controls formation and differentiation of multipotent preplacodal ectoderm progenitors from human embryonic stem cells. Dev Biol 2013:1–13.

15 Litsiou A, Hanson S, Streit A. A balance of FGF, BMP and WNT signalling positions the future placode territory in the head. Development 2005;132:4051–4062.

16 Oshima K, Shin K, Diensthuber M et al. Mechanosensitive hair cell-like cells from embryonic and induced pluripotent stem cells. Cell 2010;141:704–716.

17 Streit A. The preplacodal region: An ectodermal domain with multipotential progenitors that contribute to sense organs and cranial sensory ganglia. Int J Dev Biol 2007;461:447−461.

18 Ohyama T, Mohamed OA, Taketo MM et al. Wnt signals mediate a fate decision between otic placode and epidermis. Development 2006;133(5):865–875.

19 Park B-Y, Saint-Jeannet J-P. Hindbrain-derived Wnt and Fgf signals cooperate to specify the otic placode in Xenopus. Dev. Biol. 2009;324:108–121.

20 Freter S, Muta Y, Mak S-S et al. Progressive restriction of otic fate: The role of FGF and Wnt in resolving inner ear potential. Development 2008;135:3415–3424.

21 Camarero G, Avendano C, Fernandez-Moreno C et al. Delayed inner ear maturation and neuronal loss in postnatal Igf-1-deficient mice. J Neurosci 2001;21:7630–7641.

22 Camarero G, Leon Y, Gorospe I et al. Insulin-like growth factor 1 is required for survival of transit-amplifying neuroblasts and differentiation of otic neurons. Dev Biol 2003;262:242–253.

23 León Y, Vazquez E, Sanz C et al. Insulin-like growth factor-I regulates cell proliferation in the developing inner ear, activating glycosyl-phosphatidylinositol hydrolysis and Fos expression. Endocrinology 1995;136:3494–3503.

24 León Y, Sanz C, Frago L et al. Involvement of insulin-like growth factor-I in inner ear organogenesis and regeneration. Horm Metab Res 1999;31:126–132.

25 Liu W, Li G, Chien JS et al. Sonic hedgehog regulates otic capsule chondrogenesis and inner ear development in the mouse embryo. Dev Biol 2002;248:240–250.

26 Kondo T, Johnson S, Yoder M et al. Sonic hedgehog and retinoic acid synergistically promote sensory fate specification from bone marrow-derived pluripotent stem cells. Proc Natl Acad Sci USA 2005;102:4789–4794.

27 Bissonnette CJ, Lyass L, Bhattacharyya BJ et al. The controlled generation of functional basal forebrain cholinergic neurons from human embryonic stem cells. Stem Cells 2011;29:802–811.

28 Yao S, Chen S, Clark J et al. Long-term self-renewal and directed differentiation of human embryonic stem cells in chemically defined conditions. Proc Natl Acad Sci USA 2006;103:6907–6912.

29 Chambers SM, Qi Y, Mica Y et al. Combined small-molecule inhibition accelerates developmental timing and converts human pluripotent stem cells into nociceptors. Nat Biotechnol 2012;30:715–720.

30 Pruszak J, Sonntag K-C, Aung MH et al. Markers and methods for cell sorting of human embryonic stem cell-derived neural cell populations. Stem Cells 2008;25:2257–2268.

31 Schreiner C, Kurtz A, Bosio A et al. Sequential magnetic enrichment of NCSCs enhances peripheral neuron differentiation. MACS&MORE 2012;14:13–15.

32 Kondo T, Matsuoka AJ, Shimomura A et al. Wnt signaling promotes neuronal differentiation from mesenchymal stem cells through activation of Tlx3. Stem Cells 2011;29:836–846.

33 Kondo T, Sheets PL, Zopf DA et al. Tlx3 exerts context-dependent transcriptional regulation and promotes neuronal differentiation from embryonic stem cells. Proc Natl Acad Sci USA 2008;105:5780–5785.

34 Alves LB, Mariguela VC, Fernando M et al. Expression of osteoblastic phenotype in periodontal ligament fibroblasts cultured in three-dimensional collagen gel. J Appl Oral Sci 2015;23:206–214.

35 Miller EW, Lin JY, Frady EP et al. Optically monitoring voltage in neurons by photo-induced electron transfer through molecular wires. Proc Natl Acad Sci USA 2012;109:2114–2119.

36 Thonabulsombat C, Johansson S, Spenger C et al. Implanted embryonic sensory neurons project axons toward adult auditory brainstem neurons in roller drum and Stoppini co-cultures. Brain Res 2007;1170:48–58.

37 Novozhilova E, Olivius P, Siratirakun P et al. Neuronal differentiation and extensive migration of human neural precursor cells following co-culture with rat auditory brainstem slices. PLoS One 2013;8:e57301.

38 Berns EJ, Sur S, Pan L et al. Aligned neurite outgrowth and directed cell migration in self-assembled monodomain gels. Biomaterials 2014;35:185–195.

39 Welch BL. The generalization of 'Student's' problem when several different population variances are involved. Biometrika 1947;34:28–35.

40 Grocott T, Tambalo M, Streit A. The peripheral sensory nervous system in the vertebrate head: A gene regulatory perspective. Dev Biol 2012;370:3–23.

41 Streit A. The preplacodal region: An ectodermal domain with multipotential progenitors that contribute to sense organs and cranial sensory ganglia. Int J Dev Biol 2007;51:447–461.

42 Lleras-Forero L, Streit A. Development of the sensory nervous system in the vertebrate head: The importance of being on time. Curr Opin Genet Dev 2012;22:315–322.

43 Pirvola U, Ylikowski J. Neurotrophic factors during inner ear development. In: Romand R, Varela-Nieto I, eds. Current Topics in Developmental Biology Volume 57. Development of Auditory and Vestibular Systems-3. Molecular Development of the Inner Ear. 2nd ed. New York, NY: Elsevier, 2003:217.

44 Needham K, Hyakumura T, Gunewardene N et al. Electrophysiological properties of neurosensory progenitors derived from human embryonic stem cells. Stem Cell Res 2014;12:241–249.

45 Lu CC, Appler JM, Houseman EA et al. Developmental profiling of spiral ganglion neurons reveals insights into auditory circuit assembly. J Neurosci 2011;31:10903–10918.

46 Jones JM, Warchol ME. Expression of the Gata3 transcription factor in the acoustic ganglion of the developing avian inner ear. J Comp Neurol 2009;516:507–518.

47 McCarroll MN, Lewis ZR, Culbertson MD et al. Graded levels of Pax2a and Pax8 regulate cell differentiation during sensory placode formation. Development 2012;139:2740–2750.

48 Streit A. Extensive cell movements accompany formation of the otic placode. Dev Biol 2002;249:237–254.

49 Appler JM, Goodrich L. Connecting the ear to the brain: Molecular mechanisms of auditory circuit assembly. Prog Neurobiol 2012;93:488–508.

50 Chen W, Johnson SL, Marcotti W et al. Human fetal auditory stem cells can be expanded in vitro and differentiate into functional auditory neurons and hair cell-like cells. Stem Cells 2009;27:1196–1204.

51 Appler JM, Lu CC, Druckenbrod NR et al. Gata3 is a critical regulator of cochlear wiring. J Neurosci 2013;33:3679–3691.

52 Nayagam BA, Edge AS, Needham K et al. An in vitro model of developmental synaptogenesis using co-cultures of human neural progenitors and cochlear explants. Stem Cells Dev 2012;22:901–912.

53 Gunewardene N, Dottori M, Nayagam BA. The convergence of cochlear implantation with induced pluripotent stem cell therapy. Stem Cell Rev 2012;8:741–754.

54 Ahmed M, Xu J, Xu P-X. EYA1 and SIX1 drive the neuronal developmental program in cooperation with the SWI/SNF chromatin-remodeling complex and SOX2 in the mammalian inner ear. Development 2012;139:1965–1977.

55 Chambers S, Fasano C. Highly efficient neural conversion of human ES and iPS cells by dual inhibition of SMAD signaling. Nat Biotechnol 2009;27:275–280.

56 Eiges R, Schuldiner M, Drukker M et al. Establishment of human embryonic stem cell-transfected clones carrying a marker for undifferentiated cells. Curr Biol 2001;11:514–518.

57 Perrier AL, Tabar V, Barberi T et al. Derivation of midbrain dopamine neurons from human embryonic stem cells. Proc Natl Acad Sci USA 2004;101:12543–12548.

58 Carpenter MK, Inokuma MS, Denham J et al. Enrichment of neurons and neural precursors from human embryonic stem cells. Exp Neurol 2001;172:383–397.

59 Nistor GI, Totoiu MO, Haque N et al. Human embryonic stem cells differentiate into oligodendrocytes in high purity and myelinate after spinal cord transplantation. Glia 2005;49:385–396.

60 Kriks S, Shim J-W, Piao J et al. Floor plate-derived dopamine neurons from hESCs efficiently engraft in animal models of PD. Nature 2012;480:547–551.

61 Hoffman LM, Carpenter MK. Characterization and culture of human embryonic stem cells. Nat Biotechnol 2005;23:699–708.

62 Zhang X, Huang CT, Chen J et al. Pax6 is a human neuroectoderm cell fate determinant. Cell Stem Cell 2010;7:90–100.

63 Green SH, Bailey E, Wang Q et al. The Trk A, B, C's of Neurotrophins in the Cochlea. Anat Rec (Hoboken) 2012;295:1877–1895.

64 Ullmann U, In't Veld P, Gilles C et al. Epithelial-mesenchymal transition process in human embryonic stem cells cultured in feeder-free conditions. Mol Hum Reprod 2007;13:21–32.

65 Fritzsch B, Fariñas I, Reichardt LF. Lack of neurotrophin 3 causes losses of both classes of spiral ganglion neurons in the cochlea in a region-specific fashion. J Neurosci 1997;17:6213–6225.

66 Aburto MR, Magariños M, Leon Y et al. AKT signaling mediates IGF-I survival actions on otic neural progenitors. PLoS One 2012;7:e30790.

67 Hambright D, Park K-Y, Brooks M et al. Long-term survival and differentiation of retinal neurons derived from human embryonic stem cell lines in un-immunosuppressed mouse retina. Mol Vis 2012;18:920–936.

68 Lee KS, Zhou W, Scott-McKean JJ et al. Human sensory neurons derived from induced pluripotent stem cells support varicella-zoster virus infection. PLoS One 2012;7:e53010.

69 Flores-Otero J, Xue HZ, Davis RL. Reciprocal regulation of presynaptic and postsynaptic proteins in bipolar spiral ganglion neurons by neurotrophins. J Neurosci 2007;27:14023–14034.

70 Liu W, Kinnefors A, Boström M et al. Distribution of pejvakin in human spiral ganglion: An immunohistochemical study. Cochlear Implant Int 2013;14:225–231.

71 Li Y, Peng A, Ge S et al. MiR-204 suppresses cochlear spiral ganglion neuron survival invitro by targeting TMPRSS3. Hear Res 2014;314:60–64.

72 Benjamini Y, Hochberg Y. Controlling the false discovery rate: A practical and powerful approach to multiple testing. J R Stat Soc B 1995;57:289–300.

73 Eybalin M. Neurotransmitters and neuromodulators of the mammalian cochlea. Physiol Rev 1993;73:309–373.

74 Anniko M, Arnold W, Stigbrand T et al. The human spiral ganglion. ORL 1995;57:68–77.

75 Delmaghani S, Castillo FJ del, Michel V et al. Mutations in the gene encoding pejvakin, a newly identified protein of the afferent auditory pathway, cause DFNB59 auditory neuropathy. Nat Genet 2006;38:770–778.

76 Guipponi M, Toh M-Y, Tan J et al. An integrated genetic and functional analysis of the role of type II transmembrane serine proteases (TMPRSSs) in hearing loss. Hum Mutat 2008;29:130–141.

77 Guipponi M, Vuagniaux G, Wattenhofer M et al. The transmembrane serine protease (TMPRSS3) mutated in deafness DFNB8/10 activates the epithelial sodium channel (ENaC) in vitro. Hum Mol Genet 2002;11:2829–2836.

78 Barembaum M, Bronner-Fraser M. Spalt4 mediates invagination and otic placode gene expression in cranial ectoderm. Development 2007;134:3805–3814.

79 Bonito M Di, Narita Y, Avallone B et al. Assembly of the auditory circuitry by a Hox genetic network in the mouse brainstem. PLoS Genet 2013;9:e1003249.

80 Arenkiel BR, Tvrdik P, Gaufo GO et al. Hoxb1 functions in both motoneurons and in tissues of the periphery to establish and maintain the proper neuronal circuitry. Genes Dev 2004;18:1539–1552.

81 Narita Y, Rijli FM. Hox genes in neural patterning and circuit formation in the mouse hindbrain. In: Pourquie O, ed. Current Topics in Developmental Biology. Vol 88. 1st ed. New York, NY: Elsevier, 2009:139–167.

82 Goddard JM, Rossel M, Manley NR et al. Mice with targeted disruption of Hoxb-1 fail to form the motor nucleus of the VIIth nerve. Development 1996;122:3217–3228.

83 Gould A, Itasaki N, Krumlauf R. Initiation of rhombomeric Hoxb4 expression requires induction by somites and a retinoid pathway. Neuron 1998;21:39–51.

84 Lawoko-Kerali G, Rivolta MN, Lawlor P et al. GATA3 and NeuroD distinguish auditory and vestibular neurons during development of the mammalian inner ear. Mech Dev 2004;121:287–299.

85 Zheng JL, Helbig C, Gao WQ. Induction of cell proliferation by fibroblast and insulin-like growth factors in pure rat inner ear epithelial cell cultures. J Neurosci 1997;17:216–226.

See www.StemCellsTM.com for supporting information available online.

Stem Cells Translational Medicine published by Wiley Periodicals, Inc. on behalf of AlphaMed Press